atmosphere

MDPI

Article

Temperature and Precipitation Extremes in the Brazilian Legal Amazon: A Summary of Climatological Patterns and Detected Trends

Wanderson Luiz-Silva [1,*], Anna Carolina Fernandes Bazzanela [1,2], Claudine Pereira Dereczynski [1], Antonio Carlos Oscar-Júnior [3] and Igor Pinheiro Raupp [2]

[1] Department of Meteorology, Federal University of Rio de Janeiro, Rio de Janeiro 21941-909, Brazil; bazzanelaannacarolina@ufrj.br (A.C.F.B.); claudine.dereczynski@igeo.ufrj.br (C.P.D.)
[2] Brazilian Electric Energy Research Center (CEPEL), Rio de Janeiro 21941-911, Brazil; raupp@cepel.br
[3] Department of Geography, Rio de Janeiro State University, Rio de Janeiro 20550-900, Brazil; antonio.junior@uerj.br
* Correspondence: wanderson@igeo.ufrj.br

Abstract: The continuous understanding of extreme weather events in the Amazon is fundamental due to the importance of this biome for the regional and planetary climate system. Climate characterization and the identification of changes in the current climate can be key findings for adaptation and mitigation measures. This study examined climatology and trends in 20 climate extreme indices associated with air temperature and precipitation in the Brazilian Legal Amazon (BLA). Daily observed data, interpolated at grid points, were analyzed from 1961 to 2020. Statistical tests were employed to determine the trend's significance and magnitude. The results indicate that prolonged heat, hot days, and annual temperature records have become increasingly frequent in practically all of BLA over the last decades. Warm days and nights are increasing at approximately +11 days/decade. Heat waves have gone from 10 to 20 consecutive days on average in the 1960s to around 30–40 days in recent years. Indices associated with the intensity and frequency of extreme precipitation show a reduction, especially in the rainiest portion of the BLA, the western sector. In the east/south region of BLA, where consecutive dry days reach 100 days/year, they continue to increase at a rate of +1.5 days/decade, a fact related to the delay at the beginning of the rainy season. These aspects deserve attention since they impact local circulation, reducing the convergence of humidity not only over the BLA but also in central-southern region of Brazil.

Keywords: Amazon; climatology; climate change; climate extremes; precipitation; temperature

check for updates

Academic Editor: Masoud Rostami

Received: 27 December 2024
Revised: 11 February 2025
Accepted: 12 February 2025
Published: 16 February 2025

Citation: Luiz-Silva, W.; Bazzanela, A.C.F.; Dereczynski, C.P.; Oscar-Júnior, A.C.; Raupp, I.P. Temperature and Precipitation Extremes in the Brazilian Legal Amazon: A Summary of Climatological Patterns and Detected Trends. *Atmosphere* **2025**, *16*, 222. https://doi.org/10.3390/atmos16020222

Copyright: © 2025 by the authors. Licensee MDPI, Basel, Switzerland. This article is an open access article distributed under the terms and conditions of the Creative Commons Attribution (CC BY) license (https://creativecommons.org/licenses/by/4.0/).

1. Introduction

The general circulation of the atmosphere, as well as precipitation in South America and even in more distant places in the Northern Hemisphere, suffer a direct effect of the components of the hydrological cycle on the Amazon, especially condensation and evaporation [1,2]. In addition, the Amazon Forest biome is home to about 15% of global biodiversity, thus being biologically the wealthiest region on Earth, contributing to the biogeochemical functioning of the Earth system [3]. According to [4], the large-scale degradation of the Amazon Forest would leave a lasting negative legacy for the functioning and diversity arising from the atmosphere–biosphere interaction.

The Amazon of the coming decades may be even more vulnerable than climate models assume, since deforestation, forest fragmentation, and changes in land cover and land

use have negative ecological consequences [5,6]. This fact raises important questions about how deforestation and forest fragmentation influence regional and global climate. Several studies have investigated regional climate change associated with deforestation of the Amazon rainforest [7–9]. There is evidence that a local reduction in rainfall and an increase in air temperature occur due to deforestation of the Amazon rainforest. However, the conclusions of such studies depend on a series of parameterized processes, such as convection schemes in coupled climate models [10]. In the long term, global warming and consequent climate change receive a considerable contribution from releasing carbon into the atmosphere through deforestation and forest degradation, which are significant sources of greenhouse gas emissions into the atmosphere [11].

According to the Intergovernmental Panel on Climate Change (IPCC) [12], more frequent and severe droughts in the coming decades may affect large areas of the Amazon basin and other tropical forest formations due to the accumulation of greenhouse gases. These disturbances are caused by an unevenness in the planet's energy balance and the hydrological cycle [13]. This trend can interact synergistically with the variability of sea surface temperature anomalies, generating even more frequent and intense extreme precipitation and drought events driven by deforestation [14], as observed in 2005 [15].

It is known that the most critical mode of interannual climate variability globally, the El Niño—Southern Oscillation (ENSO) phenomenon, has a marked effect on the spatial and temporal variability of rainfall and hydrology in the Amazon [16–19]. El Niño events in 2005, 2010, 2015, and 2023, with episodes of heat waves co-occurring, caused significant impacts on the hydrological cycle of the Amazon [20–24]. Global climate change can intensify extreme episodes of drought or flooding derived from ENSO [25].

According to [26], the high precipitation deficit observed in 2015, which affected 80% of the Amazon basin—especially in the eastern portion—outlined the exceptional character of the drought episode that year. On the other hand, [27] highlights the influence of La Niña episodes on floods in the basin. The local population of the Amazon uses the rivers of the region for their subsistence, which also serves as transportation. The area's existing and planned hydroelectric reservoirs are also essential for Brazil's energy demand [28]. These activities are affected by both medium-term climate variability and long-term climate change. The intensity and extent of floods and droughts in the basin are directly related to the significant seasonal and interannual variations and the changes observed in these patterns over the decades [29,30].

Most studies on climate change in the Amazon focus on verification of trends. However, prior knowledge of the spatial characterization of climate extremes in recent decades is also essential. Research shows that, for the entire Amazon region, annual minimum, maximum, and average temperatures show upward trends, while some areas show significant decreasing trends in the region's dry season rainfall volumes [16,31–35]. According to [22], warming may intensify the severity of droughts in the future due to the reduction in precipitation and the increase in potential evapotranspiration. There is evidence that the length of the dry season in the Amazon has been increasing, thus affecting local biodiversity and river flow [16,36–38]. For research on local and regional impacts, it is fundamental that such modifications over the years are made available in detail for each region of the study area.

In this context, this work aims to structure a compendium of climatology and observed trends associated with climate extreme indices related to air temperature and precipitation in the Brazilian Legal Amazon (BLA). The BLA is a political definition attributed by the Brazilian government to the area of the Amazon rainforest belonging to Brazil (Figure 1). It is composed of nine Brazilian states: Acre (AC), Amapá (AP), Amazonas (AM), Mato Grosso (MT), Pará (PA), Tocantins (TO), Rondônia (RO), Roraima (RR), and the part of the

state of Maranhão (MA) west of the 44°W meridian. Management strategies that consider the probability of an increase in extreme weather events in line with climate variability, especially the continuous warming trend, are fundamental for the future sustainability of the Amazon rainforest and the ecosystem services it offers.

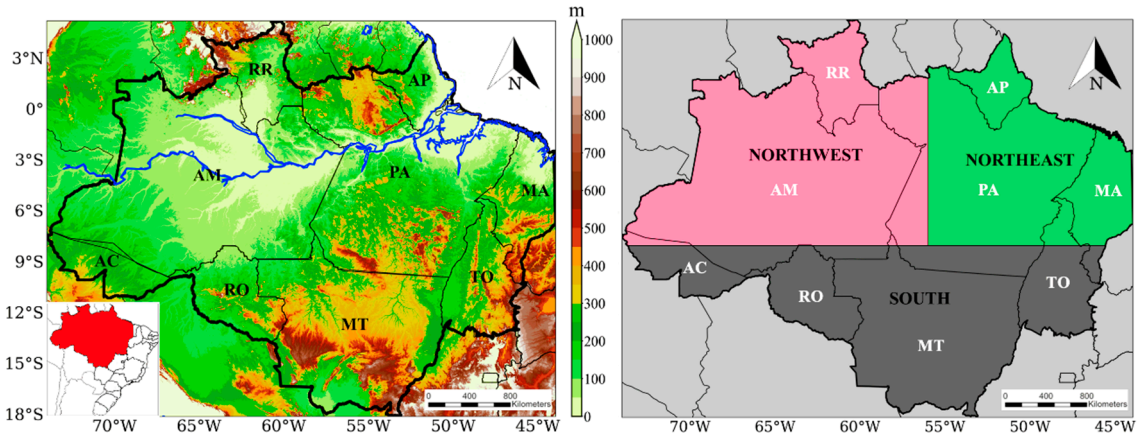


Figure 1. Brazilian Legal Amazon (BLA) region (**left**) with topography (m) and the three subdivisions of the study area (**right**): northwest (NW), northeast (NE), and south (S). The Brazilian states that compose the BLA are Acre (AC), Amapá (AP), Amazonas (AM), Maranhão (MA), Mato Grosso (MT), Pará (PA), Rondônia (RO), Roraima (RR), and Tocantins (TO).

2. Methodology

2.1. Study Area

The BLA (Figure 1) includes the hydrographic basins of the Tocantins–Araguaia and Amazon rivers and encompasses three different biomes (Amazon, Cerrado, and Pantanal). According to data from the Brazilian Institute of Geography and Statistics (IBGE), the BLA occupies an area of approximately 5 million square kilometers, accounting for 70% of the total spatial extension of the world's tropical forests. BLA has Brazil's most significant hydroelectric potential [39], which is currently close to 110 thousand MW.

The region is mainly covered by the Amazon Rainforest, the largest tropical forest in the world and home to significant biodiversity. BLA has a predominantly equatorial (or humid tropical) climate, with substantial annual rainfall accumulations, no or short dry periods, and high temperatures throughout the year [40]. Annual rainfall volumes range from 2000 to 3000 mm [19], and flooding usually occurs between December and May [41].

2.2. Observed Data

The characterization of the climate of a given region depends primarily on three factors: the quantity and quality of data available per area and the size of the time series of the variable analyzed. For a country with continental dimensions like Brazil, the information available regionally is small. This scarcity of data can be observed mainly in the country's north, northeast, and midwest regions, making it an obstacle to research aimed at the spatial detection of trends in climate extremes.

This work includes daily data on minimum and maximum air temperatures and precipitation from the Brazilian Daily Weather Gridded Data (BR-DWGD) [42]. This database was developed from the combination of information from the National Institute of Meteorology (INMET) surface meteorological stations and rainfall stations of the National Water and Basic Sanitation Agency (ANA). The data have a strong temporal coverage, covering the period from January 1961 to July 2020 (2022, for precipitation) with a spatial resolution of 0.1° latitude × 0.1° longitude. The interpolation method used is the Inverse Distance Weighted (IDW) [43]. Unfortunately for the BLA, the data density is the lowest

compared to the other Brazilian regions, with one rainfall station every 250 thousand km^2 until 2003 and one every 150 thousand km^2 in recent years. Extensive areas, such as the south of Pará, lack weather stations.

In 2021, the World Meteorological Organization (WMO) updated the climate normals to the 1991–2020 baseline period to provide the most recent data for climate information. Therefore, in this study, the period considered for air temperature climatology is 1991–2019, while for precipitation, it is 1991–2020. For trends, the entire available period is considered, that is, 1961–2019 for air temperature and 1961–2020 for precipitation.

2.3. Climate Extreme Indices

The Expert Team on Climate Change Detection and Indices (ETCCDI) of the Climatology Commission (CCl) of the World Meteorological Organization (WMO) elaborated the climate extremes indices used in this research. Twenty indices based on daily data of minimum temperature, maximum temperature, and precipitation were used (Table 1). The indicators consider extreme climate events' duration, frequency, and intensity [44,45]. Several studies in Brazil and around the world have been using these indicators of climate extremes to detect changes in the present climate [32,33,46–51] and to project changes in the future climate [32,52–55]. The *xclim* library from Python was employed to compute the extreme climate indices from the observational data. We also used Python 3.9.7 tools to structure all the figures presented in this work.

Table 1. List of climate extremes indices evaluated in this research.

Index	Definition	Unit
TMAXmean	Mean maximum temperature (TX)	°C
TMINmean	Mean minimum temperature (TN)	°C
DTR	Daily temperature range	°C
TXx	Maximum value of daily maximum temperature	°C
TXn	Minimum value of daily maximum temperature	°C
TNx	Maximum value of daily minimum temperature	°C
TNn	Minimum value of daily minimum temperature	°C
TX90p	Number of days in which TX > 90th percentile	days
TX10p	Number of days in which TX < 10th percentile	days
TN90p	Number of days TN > 90th percentile	days
TN10p	Number of days in which TN < 10th percentile	days
WSDI	Annual count of days with at least 6 consecutive days in which TX > 90th percentile	days
SU35	Annual count of days in which TX > 35 °C	days
PRCPTOT	Annual total precipitation (PRCP) on wet days (PRCP > 1 mm)	mm
R95p	Annual total precipitation when PRCP > 95th percentile	mm
RX5day	Maximum rainfall on 5 consecutive days	mm
SDII	The ratio between PRCPTOT and the number of wet days (PRCP > 1 mm)	mm/day
R30mm	Annual count of days with PRCP >= 30 mm	days
CDD	Maximum number of consecutive days with PRCP < 1 mm	days
CWD	Maximum number of consecutive days with PRCP > 1 mm	days

2.4. Statistical Trend Tests

The Mann–Kendall nonparametric statistical test analyzes the significance of indicator trends [56,57]. The null hypothesis of this test is that there is no increasing or decreasing trend in the time series. The test assumes that the succession of values occurs independently and that the probability distribution remains the same (simple random series); the data need not belong to a particular distribution. This test is an appropriate method to assess the significance of possible changes in climate series [58]. Another advantage is that its results are less affected by outlier values than other tests, as its calculation is based on the sign of differences and not directly on the values of the variable. The formula for calculating the Mann–Kendall statistical test is:

$$Z = \frac{S + u}{[VAR(S)]^{\frac{1}{2}}}, \quad (1)$$

where VAR(S) is the variance and u = −1 if S > 0; u = 0 if S = 0; and u = +1 if S < 0; thus:

$$S = \sum_{k=1}^{n-1} \sum_{j=k+1}^{n} \text{signal}(x_j - x_k), \quad (2)$$

where:

$$\begin{aligned} &\text{signal}(x_j - x_k) = 1 \text{ if } x_j - x_k > 0; \\ &\text{signal}(x_j - x_k) = 0 \text{ if } x_j - x_k = 0; \\ &\text{signal}(x_j - x_k) = -1 \text{ if } x_j - x_k < 0 \end{aligned} \quad (3)$$

and:

$$VAR(S) = \frac{1}{18}[n \cdot (n-1) \cdot (2n+5) - \sum_{p=1}^{g} t_p \cdot (t_p - 1) \cdot (2t_p + 5)]. \quad (4)$$

In Equation (2), x corresponds to the time series, ranging from k (j = k + 1) to n. The number of repeated value groups is given by g (a null difference between the compared values). The number of repeated values in each group r (to g) is represented by v in Equation (4). The trend is indicated by the Z value in Equation (1), where a positive (negative) Z means an increasing (decreasing) trend by the normal distribution. Suppose the probability (p) of the Mann–Kendall test is equal to or less than the significance level α in a bilateral test. Hence, a statistically significant trend exists, whereas a p-value greater than α confirms a nonsignificant trend. The significance level α adopted for this study was 0.05 or 5%; that is, a confidence level β of 0.95 or 95%.

Compared to other parametric techniques, the Mann–Kendall test is very robust concerning normality biases and non-stationary values in the time series. For this reason, it is widely used in long-term trend surveys [28,33,35,59,60].

The Sen's Slope test assesses the magnitude of trends in indices series. The Sen's Slope test is a nonparametric method (based upon an assumption of linear trend) used to estimate the magnitude of trends [61]. To calculate Sen's Slope, the curvatures of all value pairs in a time series are computed as:

$$SEN = \text{median}\left(\frac{x_j - x_i}{j - i}\right), \forall j > i \quad (5)$$

where xj is the indicator's value in a specific year, and xi is the value in the previous year. As Sen's Slope test is insensitive to outlier values and missing data, this test is more rigorous than the usual regression slope. It provides a more realistic measure of time series trends.

3. Results and Discussions

3.1. Climatology and Trends in Extreme Events

3.1.1. Air Temperature Extremes

Figure 2 shows the annual climatologies (1991–2019) and trends (1961–2019) of the indices associated with air temperature in the BLA. TMAXmean and TMINmean represent the average annual field of maximum and minimum temperatures, respectively, while DTR represents the average daily temperature range. Table 2 presents the trends in air temperature extremes in the NW, NE, and S regions.

Due to the high levels of solar radiation that fall on the surface of the BLA throughout the year, the air temperature is relatively high in practically its entire extension [62]. TMAXmean exhibits a very homogeneous behavior in almost all of the BLA, ranging from 32 to 33 °C, except for some stretches in the eastern sector, where it reaches 34 °C (Figure 2a). The eastern portion of the BLA has a typical tropical climate, with higher temperatures during the driest time of the year (in the austral winter). In the north of Pará and the west of Amapá, TMAXmean is lower, not exceeding 31 °C, probably due to the higher precipitation frequency in this sector. The trends observed in TMAXmean show that the eastern portion of the BLA has magnitudes of up to +0.4 °C/decade, while the western sector exhibits higher magnitudes, reaching up to +0.6 °C/decade (Figure 2b). From 1980 to 2013, [31] also observed an increased rate of +0.4 °C/decade in maximum temperature across the BLA. It is noted that the most accentuated warming in the BLA began in the 1980s (Figure 2c), with average rates of up to +0.3 °C/decade, mainly in the NW region, but also in the NE and S regions, with statistically significant rates of +0.2 °C/decade (Table 2). According to [63], suggestions for the cause of the observed changes since 1980 come from patterns in tropical Atlantic and Pacific Sea surface temperatures.

The TMINmean field presents more significant spatial heterogeneity, with a clear division between the northern and southern sectors of the study area (Figure 2d). In the south–central portion, which covers the states of Acre, Mato Grosso, and Rondônia, the TMINmean does not exceed 21 °C in most of the region, impacted significantly by the occasional cold events that occur in the region during the austral autumn and winter [64]. In the south of Mato Grosso, the mean TMINmean is below 18 °C, values that are also more influenced by the incursion of cold air masses, especially between April and September [65]. In the north–central portion of the BLA, TMINmean exceeds 22 °C, with the highest values observed in the eastern sector of Amazonas and Amapá, in the north of Pará, and Roraima. As for TMAXmean, through the analysis of the verified TMINmean trends, it is evident that there is a statistically significant warming trend in almost the entire extension of the BLA (Figure 2e). Despite the difference in TMINmean between the three BLA regions, with values about 3 °C higher in the NW and NE regions than in the S region, a clear upward trend in this index has been observed in the three regions (NW, NE, and S) over the last few years (Figure 2f). The magnitude of the TMINmean trend is greater than that of TMAXmean, reaching average rates of up to +0.4 °C/decade, especially in the NE region of BLA (Table 2). In the eastern sector of the BLA, the magnitude of the TMINmean trend is more significant than in the other areas, with some points exceeding +0.8 °C/decade. In the BLA's western and northern sectors, the TMINmean trend's magnitude is more homogeneous, around +0.4 °C/decade. As seen earlier, the sharpest upward trend of TMAXmean is observed in the western and northwestern sectors of BLA, which is the opposite signal to that observed for TMINmean.

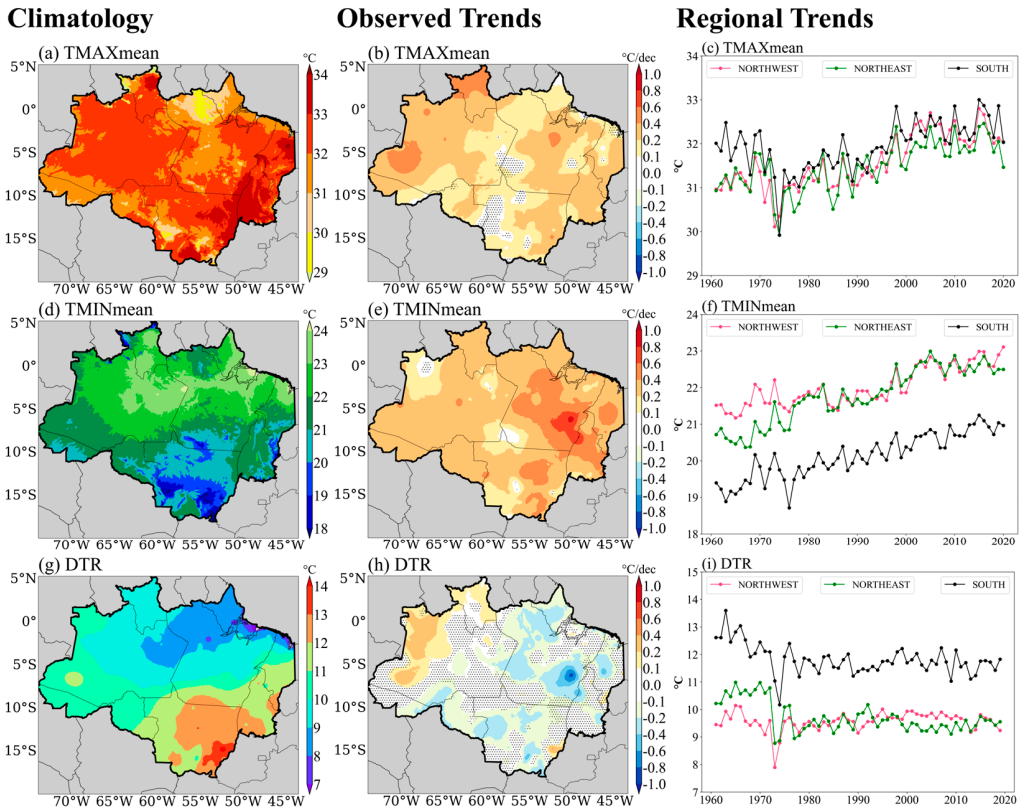


Figure 2. Climatology (**left**) for the period 1991–2019, trends (**center**), and time series in the NW, NE, and S regions of ALB (**right**) for the period 1961–2019 of the indices of climate extremes associated with air temperature: (**a**–**c**) TMAXmean, (**d**–**f**) TMINmean, and (**g**–**i**) DTR. In the observed trends, areas without dotting represent statistically significant trends at the 95% confidence level.

Table 2. Magnitudes of trends in the climate extremes indices associated with air temperature in 1961–2019 in the ALB's NW, NE, and S regions. Bold values denote statistically significant trends at the 95% confidence level.

Trends in Temperature Extremes Indices			
Indices	NW	NE	S
TMAXmean (°C/dec.)	**+0.3**	**+0.2**	**+0.2**
TMINmean (°C/dec.)	**+0.3**	**+0.4**	**+0.3**
DTR (°C/dec.)	0.0	**−0.2**	**−0.1**
TXx (°C/dec.)	**+0.3**	**+0.3**	**+0.4**
TXn (°C/dec.)	**+0.2**	**+0.1**	+0.1
TNx (°C/dec.)	**+0.3**	**+0.4**	**+0.3**
TNn (°C/dec.)	**+0.3**	**+0.5**	**+0.4**
TX90p (days/dec.)	**+10.8**	**+10.5**	**+8.1**
TN90p (days/dec.)	**+14.0**	**+11.9**	**+13.0**
TX10p (days/dec.)	**−6.8**	**−9.4**	**−3.7**
TN10p (days/dec.)	**−14.6**	**−34.0**	**−16.9**
SU35 (days/dec.)	**+4.3**	**+3.6**	**+8.0**
WSDI (days/dec.)	**+2.3**	**+2.2**	**+1.7**

In the southern and eastern sectors of the BLA, the highest values of TMAXmean and the lowest values of TMINmean are observed, resulting in high values of DTR (Figure 2g). In the north of the BLA, TMAXmean and TMINmean present their lowest and highest values due to the greater cloud cover, thus reducing the DTR value. Hence, the DTR field exhibits a north–south gradient, with lower values in the north, approximately between 8 and 9 °C, and higher values in the south, between 13 and 14 °C. In the central portion of the BLA, the magnitude of the DTR trends is smaller, in addition to presenting a few areas without statistical significance. A significant DTR reduction is observed in the central and eastern portions over −0.2 °C/decade (Figure 2h). This DTR pattern is in line with what was observed in the TMAXmean and TMINmean trends since TMINmean presents a higher upward trend than TMAXmean, thus resulting in a reduction in the mean daily temperature amplitude (Figure 2i), which reaches mean rates of up to −0.2 °C/decade in the NE region of BLA (Table 2). The only sign of a significant increase in DTR is observed in the northwestern sector of BLA, an area where the magnitudes of TMINmean trends are lower than those of TMAXmean. This increasing trend of DTR in the western Amazon had previously been verified by [36] for the period from 1980 to 2013; however, it had a slightly lower rate.

Regarding the intensity of extreme maximum temperature events (Figure 3), as observed in the climatological fields of TMAXmean, the highest values of TXx (highest annual maximum temperature) are noted in the southern and eastern sectors of the BLA. At the same time, the lowest is established in the northern and western portions (Figure 3a). In the south of Mato Grosso, TXx exceeds 38 °C, conditions that are more common between the end of winter and the beginning of the austral spring in the face of atmospheric blockages [66]. Regarding TXx trends, statistically significant warming is again observed in most of the BLA (Figure 3b). In the S region of the BLA, the warm extremes have already approached 40 °C over the last decade (Figure 3c), with an average rate of increase of +0.4 °C/decade (Table 2). A trend of a more significant rise in TXx in the BLA's west, east, and southeast sectors, reaching close to +0.8 °C/decade in some points, evidently indicating a growing trend in the daytime hot extremes. When combined with periods of drought, these extreme episodes of high maximum temperature can increase the risk of forest fires directly affecting the region's population, flora, fauna, lakes, and rivers [67].

In the same region where the highest TXx values occur (south of the BLA), the lowest TXn values (lowest maximum annual temperature) are also recorded, which are below 20 °C (Figure 3d). In the case of TXn, the lowest values are found in the southern and western portion of the study area, while the highest (>26 °C) are found in the central, northern, and eastern sectors. The low values of TXn in the south of the BLA result from the entry of masses of polar origin throughout the austral winter, which reach lower latitudes through the continent's interior, as previously mentioned. The signal is not so homogeneous regarding TXn trends, which show a decreasing trend in some regions (Figure 3e). In the state of Acre and some isolated areas of BLA, it is possible to observe a statistically significant trend of TXn reduction from −0.2 to −0.4 °C/decade. Such a reduction in TXn may be associated with increased cloudiness and precipitation in these areas. The TXn-mediated time series in the three BLA regions indicate that the annual variability is more significant in the NW and S regions than in the NE region (Figure 3f). Another point to highlight is that the trend signal does not have statistical significance in most of the BLA, except for the states of Rondônia, Roraima, and the center–north of Amazonas and Mato Grosso. The latter has the highest warming magnitude in TXn (+0.6 °C/decade).

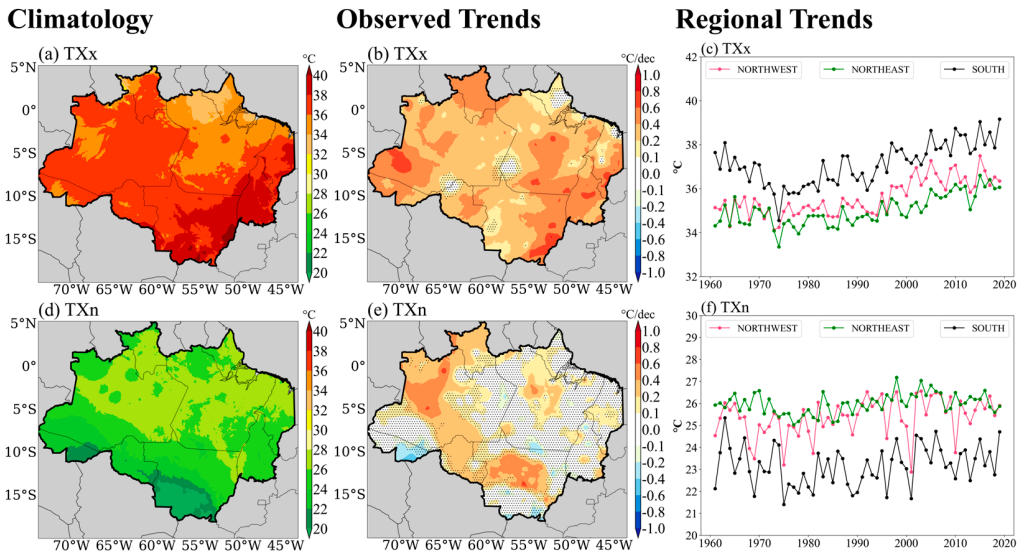


Figure 3. Climatology (**left**) for the period 1991–2019, trends (**center**), and time series in the NW, NE, and S regions of ALB (**right**) for the period 1961–2019 of the indices of climate extremes associated with air temperature: (**a**–**c**) TXx and (**d**–**f**) TXn. In the observed trends, areas without dotting represent statistically significant trends at the 95% confidence level.

Among the indices associated with the absolute extreme values of minimum temperature (Figure 4), TNx (highest annual minimum temperature) is the one that shows a more spatially uniform behavior in its climatology (Figure 4a). In most of the BLA, the values are around 24 to 26 °C. The eastern sector of the BLA (especially along the Amazon River), Roraima, northern Pará, and the central portion of Tocantins stand out, where TNx values are above 26 °C. Regarding TNx trends, there is a statistically significant warming trend in most of the BLA (Figure 4b). The warming magnitude in the BLA's west, north, and south portions is approximately +0.4 °C/decade. In contrast, in the eastern portion, this warming is more pronounced, exceeding +0.8 °C/decade in some locations, such as in the central region of Tocantins, in the southeast of Pará, and in the northeast of Mato Grosso, which encompasses the Xingu River basin, a trend also found by [34]. Such an increase in TNx over the last decades is observed in the time series shown in Figure 4c.

On the other hand, regarding climatology, TNn (lowest minimum annual temperature) is the absolute extreme index that presents the most remarkable spatial heterogeneity, with marked differences between the northern and southern sectors of the BLA (Figure 4d). In the north, the highest TNn values (>20 °C) are recorded due to its more equatorial location, while in the south, the values of this index are below 12 °C. In the extreme south of the BLA, TNn is below 10 °C in extreme cold events. The warming trend for TNn is statistically significant across the east–central BLA (Figure 4e). In addition, a trend above +1.0 °C/decade covers a portion of Mato Grosso, southeast of Pará and northwest of Tocantins. The NE region of BLA has the highest average growth rate of TNn over the last few years, with a magnitude of +0.5 °C/decade (Table 2). In this area, on average, TNn went from 17 °C in the 1960s to about 20 °C in the 2010s (Figure 4f).

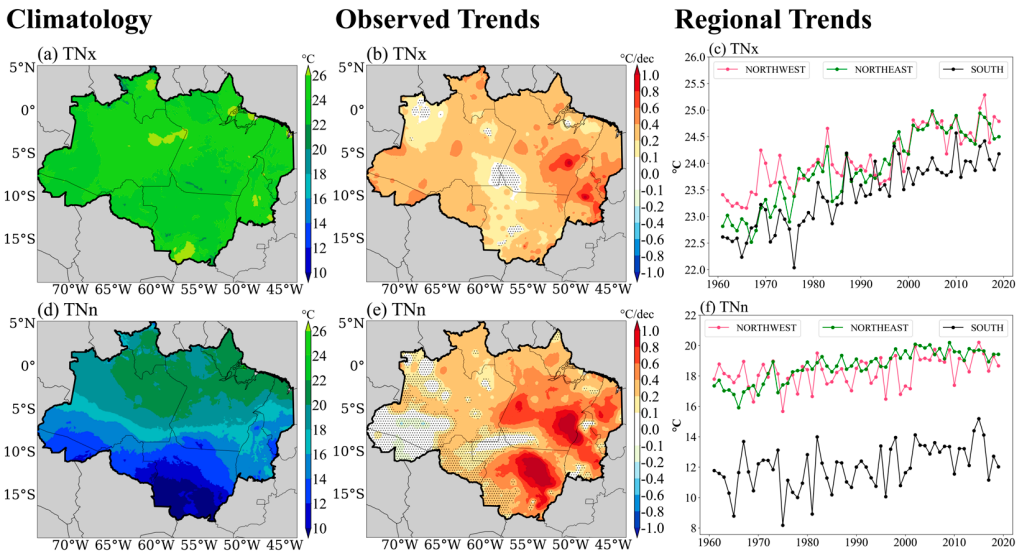


Figure 4. Climatology (**left**) for the period 1991–2019, trends (**center**), and time series in the NW, NE, and S regions of the ALB (**right**) for the period 1961–2019 of the indices of climate extremes associated with air temperature: (**a**–**c**) TNx and (**d**–**f**) TNn. In the observed trends, areas without dotting represent statistically significant trends at the 95% confidence level.

Figure 5 shows the detected trends in the frequency of extreme temperature events in the BLA. The indices associated with percentiles exhibit an upward trend in warm days and nights and a significant reduction in cold days and nights. About hot days (TX90p), an increase of more than +15 days/decade was observed in the extreme north of the study area and the central portion of Pará (Figure 5a). In recent years, TX90p has exceeded 100 days a year on average in the three BLA regions (Figure 5b). There is also a significant upward trend in the other areas, although to a lesser extent. For warm nights (TN90p), there is a more pronounced upward trend throughout the BLA, especially in the midwest and far north, exceeding the +20 days/decade mark in some regions (Figure 5c). In the last two decades, the BLA has recorded an average of more than 120 warm nights per year (Figure 5d). Among the three BLA regions, the NW region has the highest average rate of increase in the frequency of hot nights over the last few years, with a magnitude of up to +14 days/decade (Table 2). According to [68], a raised frequency of extreme temperatures can curtail human productivity and boost all-cause human mortality among disenfranchised people in the Amazon. Increased temperatures may also affect livestock and diminish crop yields, aggravated by deforestation-induced decrement in precipitation [69].

As for cold days (TX10p), there was a reduction in this index throughout BLA (Figure 5e), with the most significant decreases occurring in the central portion of the state of Pará and the northwest sector of the study area as a whole, exceeding −15 days/decade. In the three BLA regions, cold days went from 50 to 75 days per year to about 25 to 50 days per year on average in 60 years (Figure 5f). The TN10p index also stands out significantly, revealing a substantial statistically significant reduction in cold nights throughout the eastern and northern sectors of the BLA (Figure 5g). The signal magnitude in these regions is over −25 days/decade, while in the southern and western portions, the magnitude of the trend is considerably lower, staying below −15 days/decade. Cold nights in the year have decreased from approximately 150 to less than 50 nights per year on average in recent decades in the three BLA regions (Figure 5h).

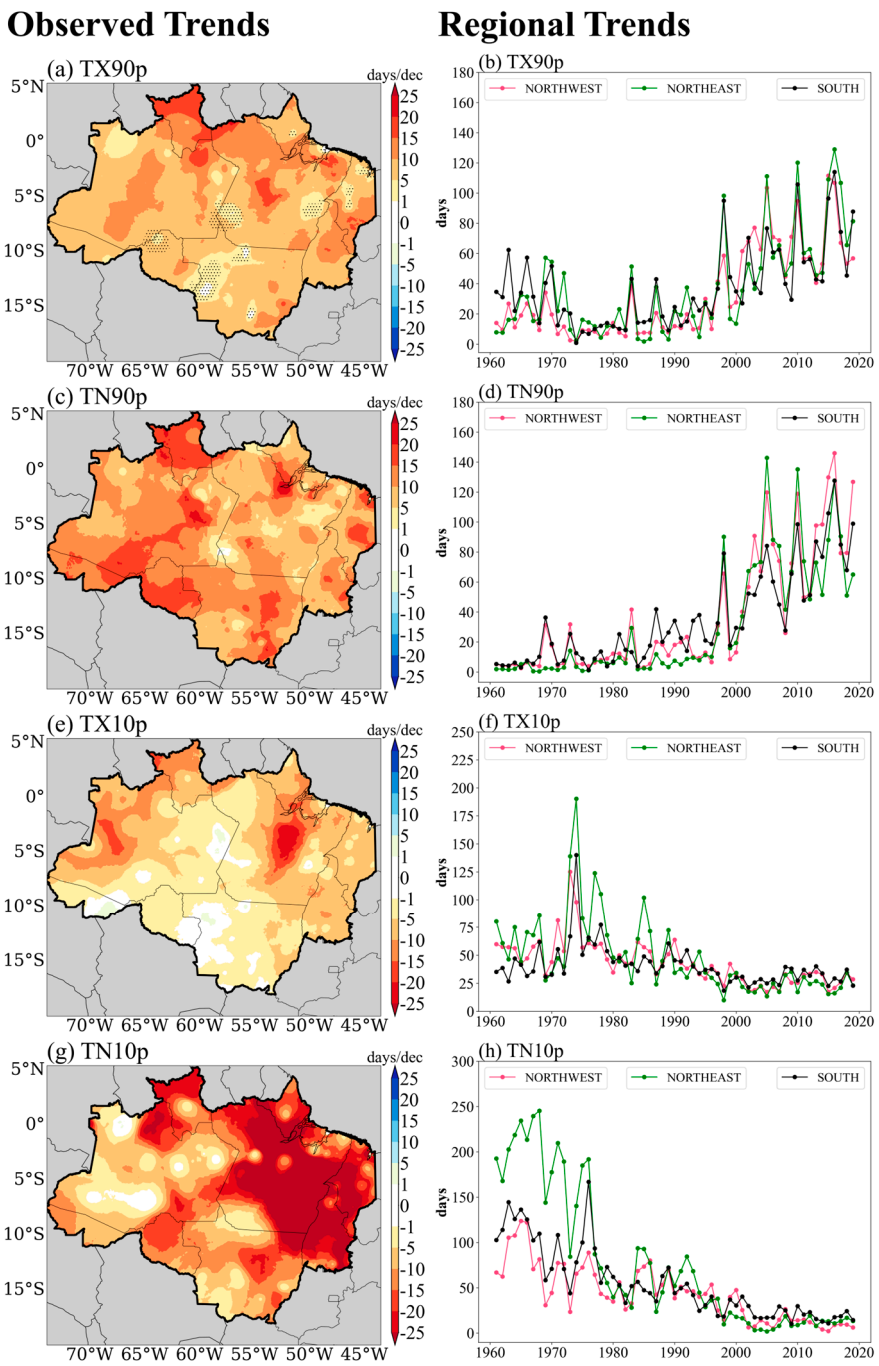


Figure 5. Trends (**left**) and time series in the NW, NE, and S regions of ALB (**right**) for the period 1961–2019 of the indices of climate extremes associated with air temperature: (**a**,**b**) TX90p, (**c**,**d**) TN90p, (**e**,**f**) TX10p, and (**g**,**h**) TN10p. In the observed trends, areas without dotting represent statistically significant trends at the 95% confidence level.

Figure 6 shows the climatology and trends of the SU35 (days with TX above 35 °C) and WSDI (duration of heat waves) indices. In the case of the SU35, the values are higher in the southeast and east sectors of the BLA (Figure 6a). Most of these hot days are recorded without precipitation, with a higher incidence of solar radiation. About a third of the year (SU35 > 100 days) registers maximum temperatures above 35 °C in the extreme south of Mato Grosso and in the state of Tocantins, which predominates during the driest time of the year (June to September). In the central–west of the BLA, the mean SU35 values do not exceed 30 days. In this region, maximum temperatures are milder due to the predominance of cloudiness and the high frequency of rainy days [19]. Figure 6b shows an upward trend

in SU35 at several points in the BLA. The magnitude of this trend is over +10 days/decade throughout the eastern sector of the study area, in the state of Rondônia, and the east part of the state of Mato Grosso, indicating a higher frequency of extremely hot days. Therefore, the S region of the BLA presents the most evident increase in SU35 (Figure 6c), reaching more than 60 days a year in recent years in this condition, at an average growth rate of +8 days/decade (Table 2).

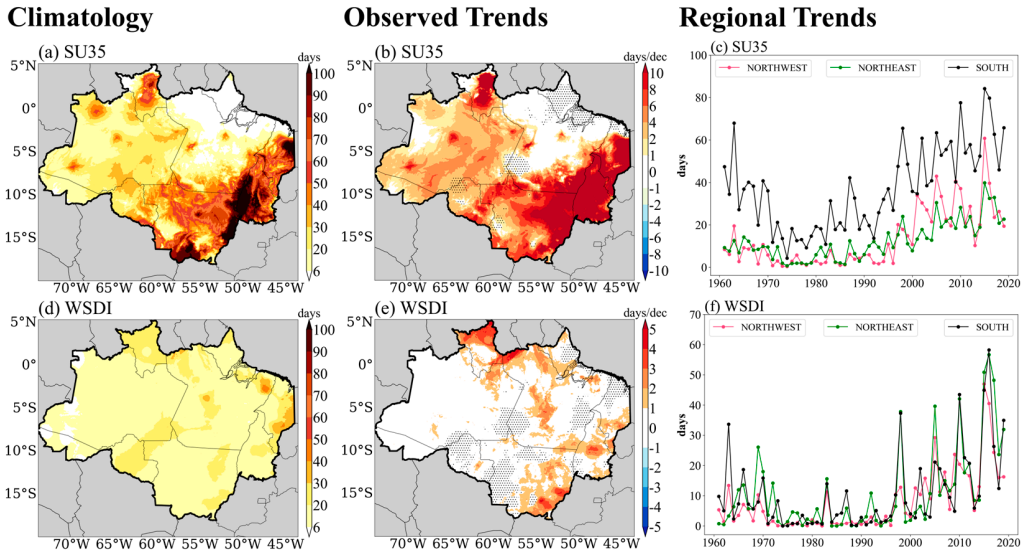


Figure 6. Climatology (**left**) for the period 1991-2019, trends (**center**), and time series in the NW, NE, and S regions of the ALB (**right**) for the period 1961-2019 of the climate extremes indices associated with air temperature: (**a**–**c**) SU35,and (**d**–**f**) WSDI. In the observed trends, areas without dotting represent statistically significant trends at the 95% confidence level.

As for WSDI (duration of heat waves), the eastern portion of the BLA experiences, on average, more than 30 days per year with very high maximum temperatures, in this case, above the 90th percentile (Figure 6d). On the other hand, in the southern, central, and northern portions of the BLA, the average WSDI values are less than 20 days. In some parts in the far west of Acre and Amazonas, the index values are less than 6 days; there are no heat waves. This variation in the index is again associated with the pattern of a higher frequency of rainy days in the western sector of the region. Similarly to the other trends, WSDI shows a statistically significant upward trend of +3 days/decade in several areas of the BLA, with special emphasis on the southeast of Mato Grosso and north of Roraima (Figure 6e). The increase in the duration of heat waves becomes more evident from the 2000s onwards in the three BLA regions (Figure 6f). [70] identified that the accretion of the northerly South Atlantic Subtropical Anticyclone (SASA) wind circulation weakens the influx of moisture to the southeastern Amazon, coinciding with the most intense heat waves recorded in this region, and ratifying the trends found in SU35 and WSDI (Figure 6), especially after the 2000s.

3.1.2. Precipitation

Figure 7 presents the annual climatologies (1991–2020) and the trends (1961–2020) of the indices of extremes related to precipitation intensity in the BLA. Regarding the PRCPTOT, it is observed that the highest annual rainfall totals are recorded in the northwest of the BLA, exceeding 3100 mm/year, while in the eastern and southern portions, the accumulated rainfall is less than 1600 mm/year (Figure 7a). This spatial difference is highlighted by the seasonality of precipitation, physiographic aspects, and atmospheric systems acting in the region. The accentuated precipitation in the northwestern part of

the study area is associated with the Intertropical Convergence Zone (ITCZ) [71], where the southeast trade winds undergo an orographic uplift over the Andes [72]. In addition, the South American Monsoon System (SAMS) begins in the northwest of the continent, involving the northwest of the BLA, with the first convective activities between the end of winter and the beginning of the austral spring [73,74]. In addition, in the north of Pará and Amapá, rainfall volumes are also significant due to the influence of the ITCZ during the late summer and early austral autumn [75,76], and their associated atmospheric disturbances, especially coastal instability lines [77].

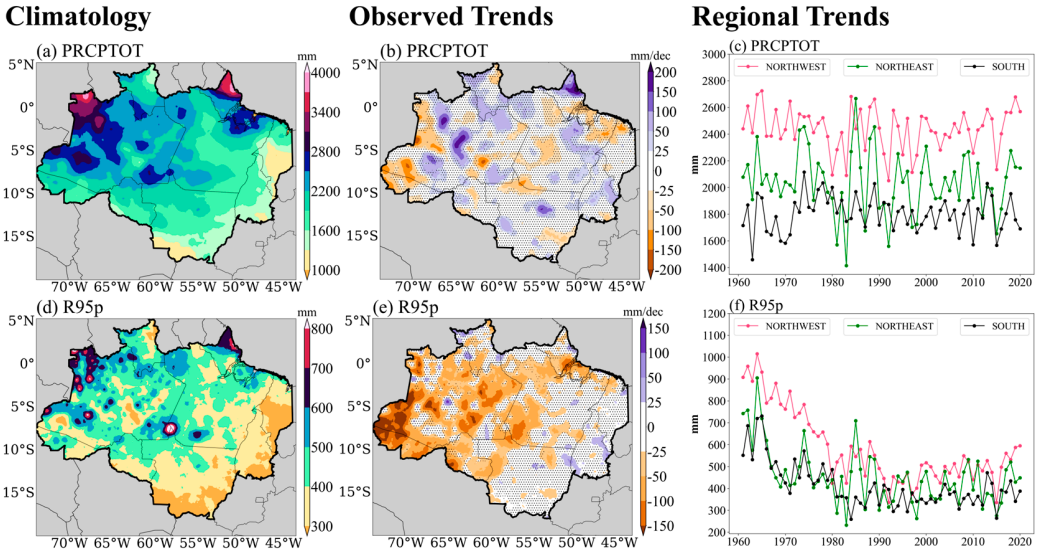


Figure 7. Climatology (**left**) for the period 1991–2020, trends (**center**), and time series in the NW, NE, and S regions of the ALB (**right**) for the period 1961–2020 of the indices of precipitation-related climate extremes: (**a**–**c**) PRCPTOT and (**d**–**f**) R95p. In the observed trends, areas without dotting represent statistically significant trends at the 95% confidence level.

Unlike temperature, the behavior of the trend is not uniform in the precipitation indices, presenting very heterogeneous trends in the BLA. In the case of PRCPTOT, isolated signs of both increase and reduction are observed over the entire length of the BLA (Figure 7b). In the state of Acre and the extreme west of the state of Amazonas, there is a reduction of more than −100 mm/decade, while in the central portion of Amazonas, there is a trend of increase in PRCPTOT greater than +100 mm/decade. This increase in the index is also significant in the north of Amapá, where the magnitude of the trend exceeds +200 mm/decade. However, when analyzing the time series in the three regions of the BLA (NW, NE, and S), it is noted that there are no statistically significant trends in PRCPTOT (Figure 7c and Table 3).

In climatological terms, the R95p index shows that the most intense precipitation events are observed at specific points in the BLA's central, western, and northern sectors (Figure 7d). The SACZ often causes heavy rain in the central portion of the study area, another characteristic system of SAMS [78,79]. In some parts of these regions, the accumulated rainfall of these events, added to the local convection, is over 800 mm/year. In the north/northeast of the BLA, the instability lines that form along the coast during the afternoon due to sea breeze circulation are responsible for the expressive volumes of rain in this area [80].

Regarding the trends of R95p, their direction is more spatially uniform than the trends of the PRCPTOT index, with a predominance of reduction in the study region (Figure 7e). The magnitude of this trend is more evident in the central–western portion of the BLA, with some areas exceeding −150 mm/decade. In the eastern and southeastern sectors of the BLA,

it is observed that some localities show a subtle upward trend, less than +75 mm/decade. The temporal evolution of R95p mediated in the three BLA regions shows a sharp decrease over the last decades (Figure 7f), especially in the NW region, where the mean rate of decline is −70.2 mm/decade (Table 3). The high frequency of El Niño events since the 1990s may be related to the reduction in heavy rainfall in this part of the Amazon [81]. In the eastern and southeastern sectors of the BLA, it is observed that some localities show a subtle upward trend, less than +25 mm/decade.

Table 3. Magnitudes of trends in the indices of climate extremes related to precipitation in 1961–2020 for the ALB's NW, NE, and S regions. Bold values represent statistically significant trends at the 95% confidence level.

Trends in Precipitation Extreme Indices			
Indices	NW	NE	S
PRCPTOT (mm/dec.)	−3.4	−11.8	−5.5
R95p (mm/dec.)	**−70.2**	**−27.3**	**−30.4**
RX5day (mm/dec.)	**−3.1**	−1.8	**−2.6**
SDII (mm/day/dec.)	**−0.4**	−0.1	**−0.1**
R30mm (days/dec.)	**−1.3**	**−0.5**	**−0.5**
CDD (days/dec.)	−0.4	+0.3	**+1.5**
CWD (days/dec.)	**+3.2**	**+2.0**	**+1.0**

In the RX5day index, associated with the maximum precipitation over five consecutive days, there is a predominance of accumulated rainfall over 120 mm/5 days in most of the BLA (Figure 8a). The only significant difference is in the north of Amapá, where this index exceeds 200 mm/5 days due to the performance of the ITCZ. Similar to the R95p index, a significant downward trend in RX5day is also evident in the western sector of BLA (Figure 8b). The magnitude of the signal is more apparent in Acre, in the southwestern sector of Amazonas, and in the extreme south of Rondônia, where it exceeds −15 mm/decade. The trend signal is quite spatially heterogeneous in the central and eastern portions of the BLA. Thus, the trend measured in the NE region is not statistically significant (Figure 8c and Table 3).

The climatology of daily precipitation intensity, represented by the SDII index (Figure 8d), presents a spatial distribution similar to that of the R95p index (Figure 7d), with higher values in the central and eastern portions of the BLA and the extreme north. In these regions, the average SDII value is around 9 to 11 mm/day, slightly higher in the north of Amapá (>14 mm/day). In general, the values of both indices are higher in the northeast and northwest edges of the study area, regions identified as hotspot areas [82,83], that is, critical points of significant biodiversity that present significant vulnerability to robust changes in climate [84]. SDII also exhibits a significant downward trend in the central–western portion of BLA, exceeding −1 mm/day per decade in some locations (Figure 8e). The analysis of the water balance in the Amazon and the simulation of deforestation and land surface processes in the BLA shows that these elements play an essential role in reducing SDII in the west of the region [85]. In the NE region of the BLA, the SDII signal is quite varied. The temporal evolution has no statistical significance (Figure 8f), with a mean magnitude of only −0.1 mm/day per decade (Table 3).

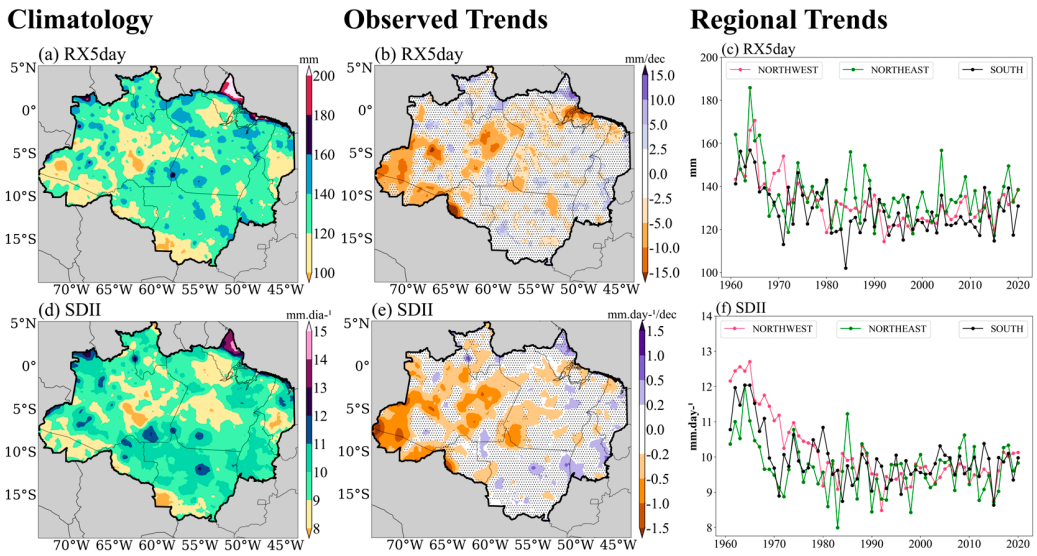


Figure 8. Climatology (**left**) for the period 1991–2020, trends (**center**), and time series in the NW, NE, and S regions of ALB (**right**) for the period 1961–2020 of the indices of precipitation-related climate extremes: (**a**–**c**) RX5day and (**d**–**f**) SDII. In the observed trends, areas without dotting represent statistically significant trends at the 95% confidence level.

Figure 9 shows the annual climatologies and trends of indices related to the frequency and duration of precipitation extremes in the BLA. The highest values of the R30mm index (days with rain above 30 mm) are found in some points of the central and northwestern portions of the BLA, as well as in the north of Amapá, exceeding 18 days a year (Figure 9a), mainly due to the ITCZ and coastal instability lines, as previously mentioned. In the eastern and southeastern sectors of the study area, the R30mm values are less than 10 days. Such frequencies of extreme rainfall are relatively low since precipitation is usually well-distributed throughout the year in the BLA. The trend of the R30mm index shows a notable negative trend in the central–west sector of BLA (Figure 9b). The magnitude of this reduction is established around −3 days/decade, being highly pronounced in all areas of BLA (Figure 9c). The local heterogeneity of trends probably happens because the forest plays a vital role in maintaining local and regional rainfall, contributing to the hydrological cycle through recycling and transporting moisture within and outside the region, depending on the land use in each area [86].

The annual climatology of the indices of consecutive dry days (CDD) and consecutive wet days (CWD) in the BLA is also shown in Figure 9. Figure 9d shows that the south and east of the BLA are the driest regions, where CDD values are highest. On average, the eastern sector of Mato Grosso and the south–central portion of Tocantins experience more than 100 consecutive days without rain in the year, indicating that the dry season is longer in this area, usually throughout the austral winter [40]. In the north and west of the study area, the average CDD is less than 20 days, where local thermodynamics contribute to more frequent convective precipitation [19]. Regarding CDD trends, there is a clear division between the east–southeast and west–northwest sectors of the BLA (Figure 9e). In the east–southeast sector, there is a significant upward trend in CDD, especially in the state of Tocantins and in the eastern sector of Mato Grosso, where the magnitude of the trend is over +4 days/decade. In the southern region of the BLA, CDD increased from the 1980s onwards, from 60 days in the 1970s to 70 days in the 2010s (Figure 9f). This region's average CDD growth rate is +1.5 days/decade (Table 3). This growth in CDD is probably associated with the increase in the dry period in the Amazon and the consequent late onset of the monsoons [87,88]. Thus, recent analyses of the tree cover distribution in this area show a change in climatic conditions that could cause critical transitions from a forest ecosystem

to a savannah ecosystem [89]. In isolated areas of the west–northwest sector, there is a reduction trend in the CDD index, although to a lesser extent, with a decrease of less than −2 days/decade.

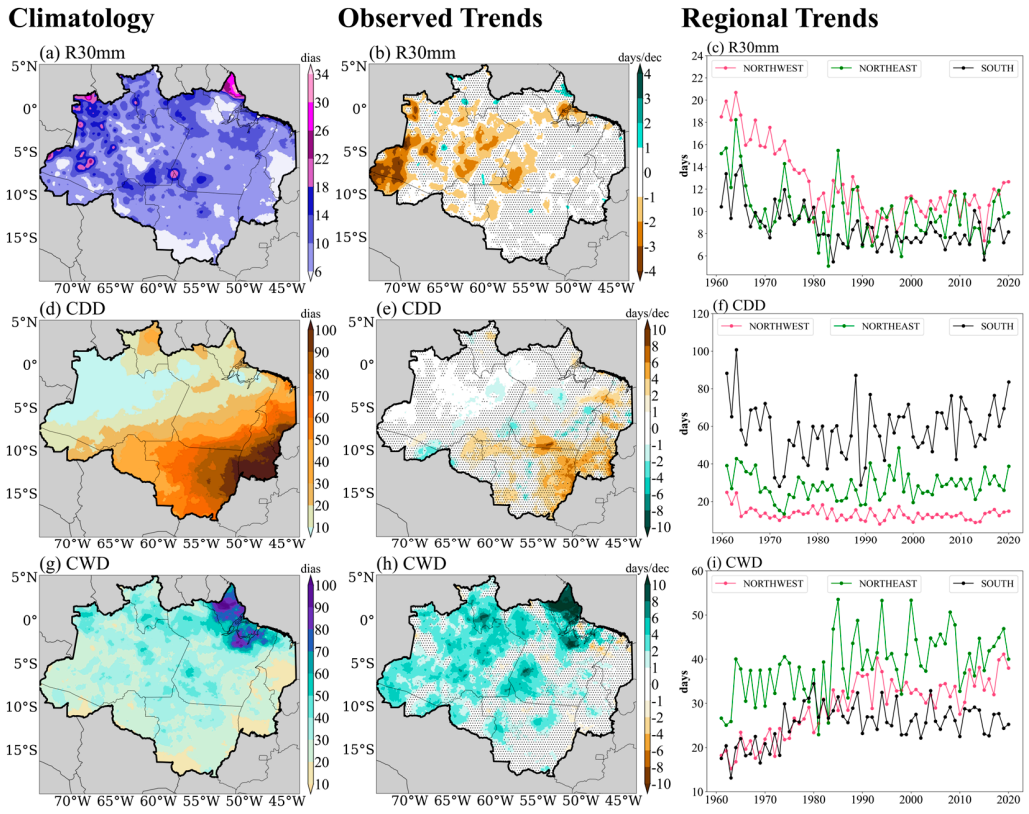


Figure 9. Climatology (**left**) for the period 1991–2020, trends (**center**), and time series in the NW, NE, and S regions (**right**) for the period 1961–2020 of the indices of precipitation-related climate extremes: (**a**–**c**) R30mm, (**d**–**f**) CDD, and (**g**–**i**) CWD. In the observed trends, areas without dotting represent statistically significant trends at the 95% confidence level.

CWD ratifies this striking characteristic of the dry period in the southeast of the BLA, since the average is a maximum of 20 consecutive days with rain per year, while in the central–northern portion, the index values are greater than 40 days (Figure 9g). In the north of Pará and the state of Amapá, the average value of the CWD is greater than 80 days during periods close to the ITCZ, which is in line with the results of other indices for this same region. In the western sector of the BLA, it is possible to observe an increase in CWD, with a magnitude greater than +2 days/decade (Figure 9h). The highest magnitudes of this index are observed in the state of Amapá, where the values exceed +10 days/decade. If consecutive wet days increase in the NW region of the BLA (Figure 9i), even with the reduction in the intensity of the precipitation extremes indices (R95p, RX5day, and SDII), this may be an indication that rainfall is better distributed, occurring with less intensity in the region.

The main trends found in the BLA over the last few decades are summarized in Figure 10. Despite the unchanged annual rainfall accumulation, there has been an accentuated decrease in the frequency and intensity of extreme precipitation events in the western portion of the BLA. On the other hand, there is an expressive growth in the duration of dry periods in the southeastern region of the Amazon, which indicates an irregular distribution of annual rainfall volumes. In addition, heat waves and extremely warm days continue to increase significantly throughout practically the entire BLA, especially in the

western, eastern, and southern sectors, which is in line with warming trends in most of Brazil [32,33,90].

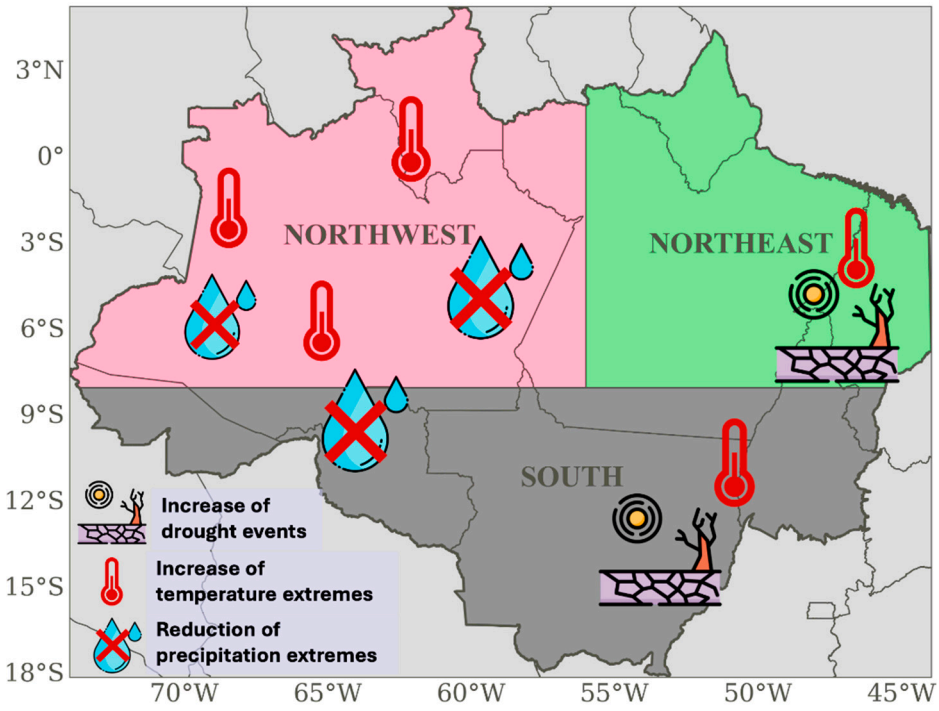


Figure 10. Summary of trends in the behavior of climate extremes related to temperature and precipitation identified over the last few years in the BLA.

4. Conclusions and Final Considerations

Detailed knowledge about extreme weather events in tropical forest regions such as the Amazon is essential due to their impacts on local ecosystems, economic activities, and the region's population. The climatological characterization of temperature and precipitation extremes presented here showed spatial and temporal patterns directly affecting such environmental and socioeconomic segments. The concentrations of greenhouse gases, such as carbon dioxide and methane, are the main contributors to the increase in average temperatures at the global and regional levels. Thus, the regional climate of the Amazon can be impacted by the rise in the concentrations of these gases, reducing the return of moisture to the atmosphere by evapotranspiration. This study compiled the climatology and detected trends in climate extremes in the BLA.

Climate extremes indices related to air temperature show a statistically significant increase in the duration, frequency, and intensity of extremely hot events in practically all of the BLA over the last few years. The frequency of days with very high maximum temperatures and annual maximum temperature records shows a sharp increase, especially in the eastern and southern portions of the BLA. In some areas, the number of days with maximum temperatures above 35 °C doubled from the end of the 20th century to the beginning of the 21st century, and today, TXx reaches 40 °C or more frequently. This warming is likely increasing evaporation and evapotranspiration in the BLA. Development in the Amazon region has gone beyond agricultural boundaries, resulting in widespread changes in land cover, especially in the southeastern portion of the BLA. In addition, studies show that the intensity of heatwaves has a greater impact than their duration concerning the health of the population in the Amazon.

The climatology of precipitation (PRCPTOT) over the BLA shows maximums in the NW region (greater than 2500 mm/year) and lower values in the eastern and southern

sectors (less than 1600 mm/year). In the wetter region of the BLA, the extremes related to intensity (R95p, RX5day, SDII) and frequency of precipitation (R30mm and CWD) show a negative trend, which implies a better rainfall distribution in this area. On the other hand, in the less rainy region, east and south of the BLA, where CDD is over 100 days/year, there is a statistically significant increase, around 4 days/decade. Such a substantial increase in dry periods usually occurs between late autumn and early austral spring. In fact, since the beginning of the twenty-first century, southern BLA has experienced a prolonged dry season related to a late onset of SAMS. Research also shows that anthropogenic forcings, such as the conversion of forests to agricultural land and deforestation, affect the length of the dry period in the region. In addition, deforestation and the increase in greenhouse gases associated with human-caused fires lead to more aerosols, which, combined with urban pollution, can modify the hydrological cycle in BLA.

The compendium of trends in climate extremes in the BLA, as carried out in this research, highlights that the rise of air masses over the Amazon can probably be inhibited by deforestation in the region, thus reducing precipitation due to lower moisture recycling. These elements impact the local circulation, reducing the convergence on the SACZ, an essential component in the delay of the rainy season in the southeast of the Amazon and the central portion of Brazil. Finally, BLA warming may further increase the severity of droughts due to increased potential evapotranspiration. Future work that considers a detailed investigation of trends in sensible and latent heat fluxes, and their relationships with temperature and precipitation extremes, may improve the quantification of climate change impacts in the Amazon.

Author Contributions: Conceptualization, W.L.-S.; Methodology, W.L.-S. and A.C.F.B.; Software, A.C.F.B.; Validation, A.C.F.B.; Formal analysis, W.L.-S.; Data curation, W.L.-S., A.C.F.B. and C.P.D.; Writing—original draft, W.L.-S.; Writing—review & editing, C.P.D. and A.C.O.-J.; Visualization, W.L.-S. and A.C.F.B.; Supervision, C.P.D. and A.C.O.-J.; Project administration, I.P.R. All authors have read and agreed to the published version of the manuscript.

Funding: This research received no external funding.

Institutional Review Board Statement: Not applicable.

Informed Consent Statement: Not applicable.

Data Availability Statement: All dataset used in this research is available in public domain: https://sites.google.com/site/alexandrecandidoxavierufes/brazilian-daily-weather-gridded-data (accessed on 10 February 2025)

Conflicts of Interest: The authors declare no conflict of interest.

References

1. Malhi, Y.; Roberts, J.T.; Betts, R.A.; Killeen, T.J.; Li, W.; Nobre, C.A. Climate change, deforestation, and the fate of the Amazon. *Science* **2008**, *319*, 169–172. [CrossRef] [PubMed]
2. Marengo, J.A.; Espinoza, J.C. Extreme seasonal droughts and floods in Amazonia: Causes, trends and impacts. *Int. J. Climatol.* **2016**, *36*, 1033–1050. [CrossRef]
3. Hubbell, S.P.; He, F.; Condit, R.; Borda-de-Água, L.; Kellner, J.; ter Steege, H. Colloquium paper: How many tree species are there in the Amazon and how many of them will go extinct? *Proc. Natl. Acad. Sci. USA* **2008**, *105*, 11498–11504. [CrossRef] [PubMed]
4. Malhi, Y.; Aragão, L.E.O.C.; GBLAraith, D.; Huntingford, C.; Fisher, R.; Zelazowski, P.; Sitch, S.; Meir, P. Exploring the likelihood and mechanism of climate-change-induced dieback of the Amazon rainforest. *Proc. Natl. Acad. Sci. USA* **2009**, *106*, 20610–20615. [CrossRef]
5. Perz, S.; Brilhante, S.; Brown, F.; Caldas, M.; Ikeda, S.; Mendoza, E.; Overdevest, C.; Reis, V.; Reyes, J.F.; Rojas, D.; et al. Road building, land use and climate change: Prospects for environmental Governance in the Amazon. *Philos. Trans. R. Soc. B* **2008**, *363*, 1889–1895. [CrossRef]

6. Silvério, D.V.; Brando, P.M.; Macedo, M.N.; Beck, P.S.A.; Bustamante, M.; Coe, M.T. Agricultural expansion dominates climate changes in southeastern Amazonia: The overlooked non-GHG forcing. *Environ. Res. Lett.* **2015**, *10*, 104015. [CrossRef]
7. Alves, L.M.; Marengo, J.A.; Fu, R.; Bombardi, R.J. Sensitivity of Amazon regional climate to deforestation. *Am. J. Clim. Change* **2017**, *6*, 75–98. [CrossRef]
8. Guimberteau, M.; Ciais, P.; Ducharne, A.; Boisier, J.P.; Aguiar, A.P.D.; Biemans, H.; De Deurwaerder, H.; Galbraith, D.; Kruijt, B.; Langerwisch, F.; et al. Impacts of future deforestation and climate change on the hydrology of the Amazon Basin: A multi-model analysis with a new set of land-cover change scenarios. *Hydrol. Earth Syst. Sci.* **2017**, *21*, 1455–1475. [CrossRef]
9. Oliveira, B.F.A.; Bottino, M.J.; Nobre, P.; Nobre, C.A. Deforestation and climate change are projected to increase heat stress risk in the Brazilian Amazon. *Commun. Earth Environ.* **2021**, *2*, 207. [CrossRef]
10. Nobre, P.; Malagutti, M.; Urbano, D.F.; Almeida, R.A.F.; Giarolla, E. Amazon deforestation and climate change in a coupled model simulation. *J. Clim.* **2009**, *22*, 5686–5697. [CrossRef]
11. Saatchi, S.S.; Harris, N.L.; Brown, S.; Lefsky, M.; Mitchard, E.T.A.; Salas, W.; Zutta, B.R.; Buermann, W.; Lewis, S.L.; Hagen, S.; et al. Benchmark map of forest carbon stocks in tropical regions across three continents. *Proc. Natl. Acad. Sci. USA* **2011**, *108*, 9899–9904. [CrossRef] [PubMed]
12. IPCC. Climate Change 2021: The Physical Science Basis. In *Contribution of Working Group I to the Sixth Assessment Report of the Intergovernmental Panel on Climate Change*; Masson-Delmotte, V.P., Zhai, A., Pirani, S.L., Connors, C., Péan, S., Berger, N., Caud, Y., Chen, L., Goldfarb, M.I., Gomis, M., Eds.; Cambridge University Press: Cambridge, UK; New York, NY, USA, 2021.
13. Betts, R.A.; Cox, P.M.; Collins, M.; Harris, P.P.; Huntingford, C.; Jones, C.D. The role of ecosystem-atmosphere interactions in simulated Amazonian precipitation decrease and forest dieback under global climate warming. *Theor. Appl. Climatol.* **2004**, *78*, 157–175. [CrossRef]
14. Brando, P.M.; Goetz, S.J.; Baccini, A.; Nepstad, D.C.; Beck, P.S.A.; Christman, M.C. Seasonal and interannual variability of climate and vegetation indices across the Amazon. *Proc. Natl. Acad. Sci. USA* **2010**, *107*, 14685–14690. [CrossRef] [PubMed]
15. Marengo, J.A.; Nobre, C.A.; Tomasella, J.; Oyama, M.D.; Oliveira, G.S.; Oliveira, R.; Camargo, H.; Alves, L.M.; Brown, I.F. The drought of Amazonia in 2005. *J. Clim.* **2008**, *21*, 495–516. [CrossRef]
16. Marengo, J.A.; Souza, C.M., Jr.; Thonicke, K.; Burton, C.; Halladay, K.; Betts, R.A.; Alves, L.M.; Soares, W.R. Changes in climate and land use over the Amazon region: Current and future variability and trends. *Front. Earth Sci.* **2018**, *6*, 228. [CrossRef]
17. Barbosa, M.L.F.; Delgado, R.C.; Andrade, C.F.; Teodoro, P.E.; Silva Junior, C.A.; Wanderley, H.S.; Capristo-Silva, G.F. Recent trends in the fire dynamics in Brazilian Legal Amazon: Interaction between the ENSO phenomenon, climate and land use. *Environ. Dev.* **2021**, *39*, 100648. [CrossRef]
18. Jimenez, J.C.; Marengo, J.A.; Alves, L.M.; Sulca, J.C.; Takahashi, K.; Ferrett, S.; Collins, M. The role of ENSO flavours and TNA on recent droughts over Amazon forests and the Northeast Brazil region. *Int. J. Climatol.* **2021**, *41*, 3761–3780. [CrossRef]
19. Luiz-Silva, W.; Oscar-Júnior, A.C.; Cavalcanti, I.F.A.; Treistman, F. An overview of precipitation Climatology in Brazil: Space-time variability of Frequency and intensity associated with atmospheric systems. *Hydrol. Sci. J.* **2021**, *66*, 289–308. [CrossRef]
20. Zeng, N.; Yoon, J.-H.; Marengo, J.A.; Subramaniam, A.; Nobre, C.A.; Mariotti, A.; Neelin, J.D. Causes and impacts of the 2005 Amazon drought. *Environ. Res. Lett.* **2008**, *3*, 014002. [CrossRef]
21. Lewis, S.L.; Brando, P.M.; Phillips, O.L.; Van Der Heijden, G.M.F.; Nepstad, D. The 2010 Amazon drought. *Science* **2011**, *331*, 554. [CrossRef]
22. Jiménez-Muñoz, J.C.; Mattar, C.; Barichivich, J.; Santamaría-Artigas, A.; Takahashi, K.; Malhi, Y.; Sobrino, J.A.; van der Schrier, G. Record-breaking warming and extreme drought in the Amazon rainforest during the course of El Niño 2015–2016. *Sci. Rep.* **2016**, *6*, 33130. [CrossRef] [PubMed]
23. Espinoza, J.C.; Jimenez, J.C.; Marengo, J.A.; Schongart, J.; Ronchail, J.; Lavado-Casimiro, W.; Ribeiro, J.V.M. The new record of drought and warmth in the Amazon in 2023 related to regional and global climatic features. *Sci. Rep.* **2024**, *14*, 8107. [CrossRef] [PubMed]
24. Lima, L.S.; Oliveira e Silva, F.E.; Anastácio, P.R.D.; Kolanski, M.M.P.; Pereira, A.C.P.; Menezes, M.S.R.; Cunha, E.L.T.P.; Macedo, M.N. Severe droughts reduce river navigability and isolate communities in the Brazilian Amazon. *Commun. Earth Environ.* **2024**, *5*, 370. [CrossRef]
25. Cai, W.; Santoso, A.; Wang, G.; Yeh, S.-W.; An, S.-I.; Cobb, K.M.; Collins, M.; Guilyardi, E.; Jin, F.-F.; Kug, J.-S.; et al. ENSO and greenhouse warming. *Nat. Clim. Change* **2015**, *5*, 849–859. [CrossRef]
26. Panisset, J.S.; Libonati, R.; Gouveia, C.M.P.; Machado-Silva, F.; França, D.A.; França, J.R.A.; Peres, L.F. Contrasting patterns of the extreme drought episodes of 2005, 2010 and 2015 in the Amazon Basin. *Int. J. Climatol.* **2018**, *38*, 1096–1104. [CrossRef]
27. Towner, J.; Ficchí, A.; Cloke, H.L.; Bazo, J.; Perez, E.C.; Stephens, E.M. Influence of ENSO and tropical Atlantic climate variability on flood characteristics in the Amazon basin. *Hydroloy Earth Syst. Sci.* **2021**, *25*, 3875–3895. [CrossRef]
28. Luiz-Silva, W.; Xavier, L.N.R.; Maceira, M.E.P.; Rotunno, O.C. Climatological and hydrological patterns and verified trends in precipitation and streamflow in the basins of Brazilian hydroelectric plants. *Theor. Appl. Climatol.* **2019**, *137*, 353–371. [CrossRef]

29. Davidson, E.A.; Araújo, A.C.; Artaxo, P.; Balch, J.K.; Brown, I.F.; Bustamante, M.M.C.; Coe, M.T.; DeFries, R.S.; Keller, M.; Longo, M.; et al. The Amazon basin in transition. *Nature* **2012**, *481*, 321–328. [CrossRef]
30. Sorribas, M.V.; Paiva, R.C.D.; Melack, J.M.; Bravo, J.M.; Jones, J.M.; Carvalho, L.; Beighley, E.; Forsberg, B.; Costa, M.H. Projections of climate change effects on discharge and inundation in the Amazon basin. *Clim. Change* **2016**, *136*, 555–570. [CrossRef]
31. Almeida, C.T.; Oliveira-Júnior, J.F.; Delgado, R.C.; Cubo, P.; Ramos, M.C. Spatiotemporal rainfall and temperature trends throughout the Brazilian Legal Amazon, 1973–2013. *Int. J. Climatol.* **2017**, *37*, 2013–2026. [CrossRef]
32. Avila-Diaz, A.; Benezoli, V.; Justino, F.; Torres, R.; Wilson, A. Assessing current and future trends of climate extremes across Brazil based on reanalyses and earth system model projections. *Clim. Dyn.* **2020**, *55*, 1403–1426. [CrossRef]
33. Regoto, P.; Dereczynski, C.P.; Chou, S.C.; Bazzanela, A.C. Observed changes in air temperature and precipitation extremes over Brazil. *Int. J. Climatol.* **2021**, *41*, 5125–5142. [CrossRef]
34. Luiz-Silva, W.; Regoto, P.; Vasconcellos, C.F.; Garcia, K.C.; Guimarães, F.B.F. A comprehensive analysis of observed and projected climate extremes of temperarure and precipitation in Belo Monte hydropower plant—Eastern Amazon, Brazil. *Int. J. Climatol.* **2022**, *42*, 9710–9729. [CrossRef]
35. Terassi, P.M.B.; Galvani, E.; Gobo, J.P.A.; Oscar-Júnior, A.C.S.; Luiz-Silva, W.; Sobral, B.S.; Gois, G.; Biffi, V.H.R. Exploring climate extremes in Brazil's Legal Amazon. *Stoch. Environ. Res. Risk Assess.* **2024**, *38*, 1403–1422. [CrossRef]
36. Silva, P.E.; Santos e Silva, C.M.; Spyrides, M.H.C.; Andrade, L.M.B. Precipitation and air temperature extremes in the Amazon and northeast Brazil. *Int. J. Climatol.* **2019**, *39*, 579–595. [CrossRef]
37. Agudelo, J.; Espinoza, J.C.; Junquas, C.; Arias, P.A.; Sierra, J.P.; Olmo, M.E. Future projections of low-level atmospheric circulation patterns over south tropical South America: Impacts on precipitation and Amazon dry season length. *J. Geophys. Res. Atmos.* **2023**, *128*, e2023JD038658. [CrossRef]
38. Sierra, J.P.; Espinoza, J.C.; Junquas, C.; Wongchuig, S.; Polcher, J.; Moron, V.; Fita, L.; Arias, P.A.; Schrapffer, A.; Pennel, R. Impacts of land-surface heterogeneities and Amazonian deforestation on the wet season onset in southern Amazon. *Clim. Dyn.* **2023**, *61*, 4867–4898. [CrossRef]
39. Soito, J.L.S.; Freitas, M.A.V. Amazon and the expansion of hydropower in Brazil: Vulnerability, impacts and possibilities for adaptation to global climate change. *Renew. Sustain. Energy Rev.* **2011**, *15*, 3165–3177. [CrossRef]
40. Alvares, C.A.; Stape, J.L.; Sentelhas, P.C.; Gonçalves, J.L.M.; Sparovek, G. Köppen's climate classification map for Brazil. *Meteorol. Z.* **2013**, *22*, 711–728. [CrossRef]
41. Latrubesse, E.M.; Arima, E.Y.; Dunne, T.; Park, E.; Baker, V.R.; d'Horta, F.M.; Wight, C.; Wittmann, F.; Zuanon, J.; Baker, P.A.; et al. Damming the rivers of the Amazon basin. *Nature* **2017**, *546*, 363–369. [CrossRef]
42. Xavier, A.C.; Scanlon, B.R.; King, C.W.; Alves, A.I. New improved Brazilian daily weather gridded data (1961–2020). *Int. J. Climatol.* **2022**, *42*, 8390–8404. [CrossRef]
43. Borges, P.A.; Franke, J.; Anunciação, Y.M.T.; Weiss, H.; Bernhofer, C. Comparison of spatial interpolation methods for the estimation of precipitation distribution in Distrito Federal, Brazil. *Theor. Appl. Climatol.* **2016**, *123*, 335–348. [CrossRef]
44. Karl, T.R.; Nicholls, N.; Ghazi, A. CLIVAR/GCOS/WMO workshop on indices and indicators for climate extremes: Workshop summary. *Clim. Change* **1999**, *42*, 3–7. [CrossRef]
45. Frich, P.; Alexander, L.V.; Della-Marta, P.; Gleason, B.; Haylock, M.; Klein Tank, A.M.G.; Peterson, T. Observed coherent changes in climatic extremes during the 2nd half of the 20th century. *Clim. Res.* **2002**, *19*, 193–212. [CrossRef]
46. Dereczynski, C.P.; Chou, S.C.; Lyra, A.; Sondermann, M.; Regoto, P.; Tavares, P.; Chagas, D.; Gomes, J.L.; Rodrigues, D.C.; Skansi, M.M. Downscaling of climate extremes over South America—Part I: Model evaluation in the reference climate. *Weather Clim. Extrem.* **2020**, *29*, 100273. [CrossRef]
47. Dunn, R.J.H.; Alexander, L.V.; Donat, M.G.; Zhang, X.; Bador, M.; Herold, N.; Lippmann, T.; Allan, R.; Aguilar, E.; Barry, A.A.; et al. Development of an updated global land in situ-based data det of temperature and precipitation extremes: HadEX3. *JGR Atmos.* **2020**, *125*, e2019JD032263. [CrossRef]
48. Luiz-Silva, W.; Silva, F.P.; Dereczynski, C.P.; França, J.R.A. Towards a link between climate extremes and thermodynamic patterns in the city of Rio de Janeiro-Brazil: Climatological aspects and identified changes. *J. Geosci. Environ. Prot.* **2023**, *11*, 131–160. [CrossRef]
49. Kara, Y.; Yavuz, V.; Temiz, C.; Lupo, A.R. Exploring spatio-temporal precipitation variations in Istanbul: Trends and patterns from five stations across two continents. *Atmosphere* **2024**, *15*, 539. [CrossRef]
50. Santos, A.L.M.; Gonçalves, W.A.; Andrade, L.M.B.; Rodrigues, D.T.; Batista, F.F.; Lima, G.C.; Silva, C.M.S. Space-time characterization ox extreme precipitation indices for the semiarid region of Brazil. *Climate* **2024**, *12*, 43. [CrossRef]
51. Yang, Y.; Chang, W. Analysis of spatial and temporal distribution and changes in extreme climate events in Northwest China from 1960 to 2021: A case study of Xinjiang. *Sustainability* **2024**, *16*, 4960. [CrossRef]
52. Li, C.; Zwiers, F.; Zhang, X.; Li, G.; Sun, Y.; Wehner, M. Changes in annual extremes of daily temperature and precipitation in CMIP6 models. *J. Clim.* **2021**, *34*, 3441–3460. [CrossRef]

53. Medeiros, J.F.; Oliveira, C.P.; Avila-Diaz, A. Evaluation of extreme precipitation climate indices and their projected changes for Brazil: From CMIP3 to CMIP6. *Weather Clim. Extrem.* **2022**, *38*, 100511. [CrossRef]
54. Reboita, M.S.; Kuki, C.A.C.; Marrafon, V.H.; Souza, C.A.; Ferreira, G.W.S.; Teodoro, T.; Lima, J.W.M. South America climate change revealed through climate indices projected by GCMs and Eta-RCM ensembles. *Clim. Dyn.* **2022**, *58*, 459–485. [CrossRef]
55. Veiga, S.F.; Nobre, P.; Giarolla, E.; Capistrano, V.B.; Silva, M.B., Jr.; Casagrande, F.; Soares, H.C.; Kubota, P.Y.; Figueroa, S.N.; Bottino, M.J.; et al. Climate change over South America simulated by the Brazilian Earth system model under RCP4.5 and RCP8.5 scenarios. *J. S. Am. Earth Sci.* **2023**, *131*, 104598. [CrossRef]
56. Mann, H.B. Non-parametric tests against trend. *Econometrica* **1945**, *13*, 245–259. [CrossRef]
57. Kendall, M.A.; Stuart, A. *The Advanced Theory of Statistics*; Charles Griffin: London, UK, 1967.
58. Sneyers, R. On the statistical analysis of series of observations. *World Meteorol. Organ.* **1990**, *415*, 192.
59. Zilli, M.T.; Carvalho, L.M.V.; Liebmann, B.; Silva Dias, M.A. A comprehensive analysis of trends in extreme precipitation over southeastern coast of Brazil. *Int. J. Climatol.* **2017**, *37*, 2269–2279. [CrossRef]
60. Costa, R.L.; Baptista, G.M.M.; Gomes, H.B.; Silva, F.D.S.; Rocha Júnior, R.L.; Salvador, M.A.; Herdies, D.L. Analysis of climate extremes indices over northeast Brazil from 1961 to 2014. *Weather Clim. Extrem.* **2020**, *28*, 100254. [CrossRef]
61. Sen, P.K. Estimates of the regression coefficient based on Kendall's tau. *J. Am. Stat. Assoc.* **1968**, *63*, 1379–1389. [CrossRef]
62. Marengo, J.A. On the hydrological cycle of the Amazon basin: A historical review and current state-of-the-art. *Rev. Bras. Meteorol.* **2006**, *21*, 1–19.
63. Gloor, M.; Barichivich, J.; Ziv, G.; Brienen, R.; Schöngart, J.; Peylin, P.; Cintra, B.B.L.; Feldpausch, T.; Phillips, O.; Baker, J. Recent Amazon climate as background for possible ongoing and future changes of Amazon humid forests. *Glob. Biogeochem. Cycles* **2015**, *29*, 1384–1399. [CrossRef]
64. Ricarte, R.M.D.; Herdies, D.L.; Barbosa, T.F. Patterns of atmospheric circulation associated with cold outbreaks in southern Amazonia. *Meteorol. Appl.* **2015**, *22*, 129–140. [CrossRef]
65. Escobar, G.C.J.; Vaz, J.C.M.; Reboita, M.S. Surface atmospheric circulation associated with "friagens" in central-west Brazil. *Anuário Do Inst. De Geociências—UFRJ* **2019**, *42*, 241–254. [CrossRef]
66. Marengo, J.A.; Ambrizzi, T.; Barreto, N.; Cunha, A.P.; Ramos, A.M.; Skansi, M.; Carpio, J.M.; Salinas, R. The heat wave of October 2020 in central South America. *Int. J. Climatol.* **2022**, *42*, 2281–2298. [CrossRef]
67. Doughty, C.E.; Metcalfe, D.B.; Girardin, C.A.J.; Amézquita, F.F.; Cabrera, D.G.; Huasco, W.H.; Silva-Espejo, J.E.; Araujo-Murakami, A.; Costa, M.C.; Rocha, W.; et al. Drought impact on forest carbon dynamics and fluxes in Amazonia. *Nature* **2015**, *519*, 78–82. [CrossRef]
68. Butt, E.W.; Baker, J.C.A.; Bezerra, F.G.S.; von Randow, C.; Aguiar, A.P.D.; Spracklen, D.V. Amazon deforestation causes strong regional warming. *Proc. Natl. Acad. Sci. USA* **2023**, *120*, e2309123120. [CrossRef] [PubMed]
69. Flach, R.; Abrahão, G.; Bryant, B.; Scarabello, M.; Soterroni, A.C.; Ramos, F.M.; Valin, H.; Obersteiner, M.; Cohn, A.S. Conserving the Cerrado and Amazon biomes of Brazil protects the soy economy from damaging warming. *World Dev.* **2021**, *146*, 105582. [CrossRef]
70. Costa, D.F.; Gomes, H.B.; Silva, M.C.L.; Zhou, L. The most extreme heat waves in Amazonia happened under extreme dryness. *Clim. Dyn.* **2022**, *59*, 281–295. [CrossRef]
71. Schneider, T.; Bischoff, T.; Haug, G.H. Migrations and dynamics of the intertropical convergence zone. *Nature* **2014**, *513*, 45–53. [CrossRef]
72. Insel, N.; Poulsen, C.J.; Ehlers, T.A. Influence of the Andes Mountains on South American moisture transport, convection, and precipitation. *Clim. Dyn.* **2010**, *35*, 1477–1492. [CrossRef]
73. Gan, M.A.; Kousky, V.E.; Ropelewski, C.F. The South America monsoon circulation and its relationship to rainfall over west-central Brazil. *J. Clim.* **2004**, *17*, 47–66. [CrossRef]
74. Marengo, J.A.; Liebmann, B.; Grimm, A.M.; Misra, V.; Silva Dias, P.L.; Cavalcanti, I.F.A.; Carvalho, L.M.V.; Berbery, E.H.; Ambrizzi, T.; Vera, C.S.; et al. Recent developments on the South American monsoon system. *Int. J. Climatol.* **2012**, *32*, 1–21. [CrossRef]
75. Fu, R.; Dickinson, R.E.; Chen, M.; Wang, H. How do tropical sea surface temperatures influence the seasonal distribution of precipitation in the Equatorial Amazon? *J. Clim.* **2001**, *14*, 4003–4026. [CrossRef]
76. Souza, E.B.; Kayano, M.T.; Ambrizzi, T. Intraseasonal and submonthly variability over the Eastern Amazon and Northeast Brazil during the autumn rainy season. *Theor. Appl. Climatol.* **2005**, *81*, 177–191. [CrossRef]
77. Sousa, A.C.; Candido, L.A.; Satyamurty, P. Convective cloud clusters and squall lines along the coastal Amazon. *Mon. Weather Rev.* **2021**, *149*, 3589–3608. [CrossRef]
78. Robertson, A.W.; Mechoso, C.R. Interannual and interdecadal variability of the South Atlantic Convergence Zone. *Mon. Weather Rev.* **2000**, *128*, 2947–2957. [CrossRef]
79. Carvalho, L.M.V.; Jones, C.; Liebmann, B. The South Atlantic Convergence Zone: Intensity, form, persistence, and relationships with intraseasonal to interannual activity and extreme rainfall. *J. Clim.* **2004**, *17*, 88–108. [CrossRef]

80. Alcântara, C.R.; Silva Dias, M.A.F.; Souza, E.P.; Cohen, J.C.P. Verification of the role of the low level jets in Amazon squall lines. *Atmos. Res.* **2011**, *100*, 36–44. [CrossRef]
81. Shimizu, M.H.; Ambrizzi, T.; Liebmann, B. Extreme precipitation events and their relationship with ENSO and MJO phases over northern South America. *Int. J. Climatol.* **2017**, *37*, 2977–2989. [CrossRef]
82. Espinoza, J.C.; Chavez, S.; Ronchail, J.; Junquas, C.; Takahashi, K.; Lavado-Casimiro, W. Rainfall hotspots over the southern tropical Andes: Spatial distribution, rainfall intensity, and relations with large-scale atmospheric circulation. *Water Resour. Res.* **2015**, *51*, 3459–3475. [CrossRef]
83. Chavez, S.P.; Takahashi, K. Orographic rainfall hot spots in the Andes-Amazon transition according to the TRMM precipitation radar and in situ data. *JGR Atmos.* **2017**, *122*, 5870–5882. [CrossRef]
84. Sherbinin, A. Climate change hotspots mapping: What have we learned? *Clim. Change* **2014**, *123*, 23–37. [CrossRef]
85. Llopart, M.; Reboita, M.S.; Coppola, E.; Giorgi, F.; Rocha, R.P.; Souza, D.O. Land use change over the Amazon Forest and its impacts on the local climate. *Water* **2018**, *10*, 149. [CrossRef]
86. Aguiar, A.P.D.; Vieira, I.C.G.; Assis, T.O.; Dalla-Nora, E.L.; Toledo, P.M.; Santos-Junior, R.A.O.; Batistella, M.; Coelho, A.S.; Savaget, E.K.; Aragão, L.E.O.C.; et al. Land use change emission scenarios: Anticipating a forest transition process in the Brazilian Amazon. *Glob. Change Biol.* **2016**, *22*, 1821–1840. [CrossRef] [PubMed]
87. Pascale, S.; Carvalho, L.M.V.; Adams, D.K.; Castro, C.L.; Cavalcanti, I.F.A. Current and future variations of the monsoons of the Americas in a warming climate. *Curr. Clim. Change Rep.* **2019**, *5*, 125–144. [CrossRef]
88. Bombardi, R.J.; Moron, V.; Goodnight, J.S. Detection, variability, and predictability of monsoon onset and withdrawal dates: A review. *Int. J. Climatol.* **2020**, *40*, 641–667. [CrossRef]
89. Staal, A.; Dekker, S.C.; Hirota, M.; van Nes, E.H. Synergistic effects of drougth and deforestation on the resilience of the south-eastern Amazon rainforest. *Ecol. Complex.* **2015**, *22*, 65–75. [CrossRef]
90. Curado, L.F.A.; Paulo, S.R.; Paulo, I.J.C.; Maionchi, D.O.; Silva, H.J.A.; Costa, R.O.; Silva, I.M.C.B.; Marques, J.B.; Lima, A.M.S.; Rodrigues, T.R. Trends and patterns of daily maximum, minimum and mean temperature in Brazil from 2000 to 2020. *Climate* **2023**, *11*, 168. [CrossRef]

Disclaimer/Publisher's Note: The statements, opinions and data contained in all publications are solely those of the individual author(s) and contributor(s) and not of MDPI and/or the editor(s). MDPI and/or the editor(s) disclaim responsibility for any injury to people or property resulting from any ideas, methods, instructions or products referred to in the content.